PHYSICAL REVIEW E **70**, 010901(R) (2004)

Sorting mesoscopic objects with periodic potential landscapes: Optical fractionation

K. Ladavac, K. Kasza, and D. G. Grier*

Department of Physics, James Franck Institute and Institute for Biophysical Dynamics, The University of Chicago, Chicago, Illinois 60637, USA

(Received 17 June 2003; revised manuscript received 22 March 2004; published 20 July 2004)

Viscously damped objects driven through a periodically modulated potential energy landscape can become kinetically locked in to commensurate directions through the landscape, and thus can be deflected away from the driving direction. We demonstrate that the threshold for an object to become kinetically locked in to an array can depend exceptionally strongly on its size. When implemented with an array of holographic optical tweezers, this process provides the basis for a continuous and continuously optimized sorting technique for mesoscopic objects called "optical fractionation."

DOI: 10.1103/PhysRevE.70.010901 PACS number(s): 87.80.Cc, 33.80.Ps, 05.60.Cd, 82.70.Dd

Many natural and technologically important processes involve classical transport of small objects through modulated potential energy landscapes. While the generic behavior of modulated transport is well understood in one dimension [1], fundamental questions remain for higher dimensions. Colloidal particles flowing through arrays of optical tweezers [2,3] provide a uniquely accessible experimental archetype for this class of problems. Experiments on transport through square arrays have revealed a devil's staircase hierarchy of kinetically locked-in states as a function of orientation [4]. Within each locked-in state, particles select commensurate paths through the array independent of the driving direction. The ability to selectively deflect one fraction out of a flowing mixture was predicted [4] to be useful for sorting and purifying mesoscopic samples. Here, we describe a practical implementation of this process, which we term optical fractionation. Analyzing the kinematics of optical fractionation further reveals that the threshold for kinetic lock-in can depend *exponentially* on size.

Optical fractionation exploits a competition between optical gradient forces exerted by optical traps [2] and an externally applied force, as shown in Fig. 1. A driven particle's trajectory can be deflected enough by an encounter with one trap to pass into the domain of the next, and so on down the line. Such a trajectory is said to be kinetically locked-in to the array. Optical fractionation's selectivity emerges because objects with different sizes, shapes or compositions can experience substantially different potential energy landscapes in the same light field; periodicity emphasizes these differences. Objects that escape from the array flow away in the driving direction, while locked-in objects can be deflected. The two resulting fractions can be collected in separate microfluidic channels downstream.

To demonstrate optical fractionation in practice, we studied the transport of water-borne colloidal particles flowing past a linear array of holographic optical tweezers [3]. The colloidal suspension was confined to a 4 mm$\times$0.7 mm $\times$40 μm glass channel formed by bonding the edges of two glass cover slips. Capillary forces at the channel's inlet were used to create a flow of about 60 μm/s along the midplane. This flow carried a mixture of monodisperse silica spheres of radius $a_1=0.79$ μm (Duke Scientific Lot No. 24169) and $a_2=0.5$ μm (Duke Scientific Lot No. 19057), which can be distinguished visually and tracked to within 30 nm in the plane at 1/60 s intervals using digital video microscopy [5].

Colloidal silica spheres are roughly twice as dense as water and settle into a monolayer just above the channel's lower wall, with the smaller spheres floating about 1 μm higher. Given the Poisseuille flow profile in the channel, the larger spheres travel slower, with a mean speed of $u_1=13\pm2$ μm/s, compared with the smaller spheres' $u_2=17\pm9$ μm/s. The associated driving force, $\boldsymbol{F}_j=\gamma_j\boldsymbol{u}_j$, is characterized by a size-dependent drag coefficient, γ_j, modified by proximity to surfaces [6].

Twelve discrete optical tweezers were arranged in a line with center-to-center spacing $b=3.6\pm0.1$ μm oriented at $\theta=12.0°\pm0.5°$ with respect to the flow. Each trap was powered by 1.7 ± 0.8 mW of laser light at 532 nm, which slightly exceeded the empirically determined lock-in threshold for the larger spheres, given θ and b. Each trap can capture

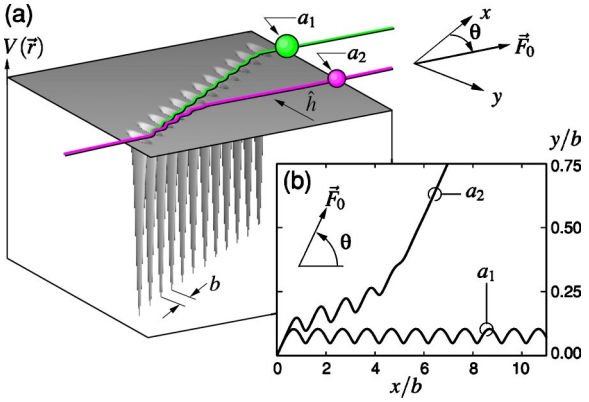

FIG. 1. Principle of optical fractionation. (a) Different types of particles are driven by external force $\boldsymbol{F}_0$ through an array of optical traps inclined at angle θ. Strongly interacting particles (a_1) are deflected by the array while the others (a_2) are not. (b) Trajectories for large ($a_1=0.79$ μm) and small ($a_2=0.5$ μm) spheres calculated with Eq. (5) for experimental conditions described in the text.

*Present address: Department of Physics, New York University, New York, NY 10003, USA.

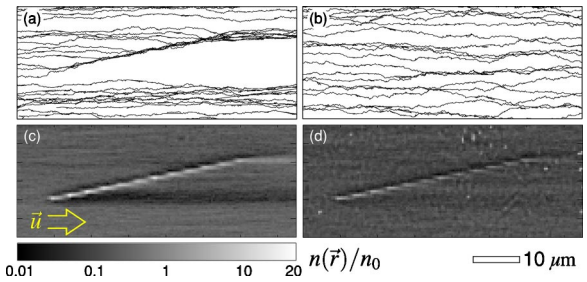

FIG. 2. Optical fractionation of bidisperse silica spheres. (a) Representative trajectories for $a_1=0.79$ μm at 1/60 s intervals. (b) Trajectories for $a_2=0.50$ μm obtained simultaneously. (c) Time-averaged areal density $n_1(\boldsymbol{r})$ for a_1 relative to the mean, n_0. Data compiled from 30 000 trajectories. (d) Simultaneously acquired data for 0.50 μm radius spheres compiled from 45 000 trajectories. The color bar indicates n_i/n_0 for both data sets, and the scale bar denotes 10 μm for all four panels.

either type of sphere in the absence of flow. The trapping plane was adjusted to minimize out-of-plane motions, so that the system is effectively two-dimensional for both populations. Although this is useful for illustrative purposes, optical fractionation also works in thick samples with three-dimensional trap arrays.

The trajectories in Figs. 2(a) and 2(b) demonstrate that the larger spheres are indeed systematically deflected by the array of traps, while the smaller spheres are not. Consequently, the array creates a shadow in the distribution of large spheres into which the small spheres can flow. Because the purification of small spheres and concentration of large results from lateral deflection, this optical fractionation process can proceed continuously, in contrast to most competing techniques [7].

Figures 2(c) and 2(d) show statistics compiled from tens of thousands of trajectories. Here, we plot the two populations' time-averaged areal densities $n_j(\boldsymbol{r})$ normalized by their means. The separation's quality is assessed in Fig. 3 with $\mathcal{Q}(\boldsymbol{r})\equiv[n_1(\boldsymbol{r})-n_2(\boldsymbol{r})]/[n_1(\boldsymbol{r})+n_2(\boldsymbol{r})]$, which reaches unity in regions containing only large spheres, and minus one in regions with only small spheres. A transverse section taken along line A in Fig. 3(a) and plotted as squares in Fig. 3(b) reveals a thoroughly mixed sample with $\mathcal{Q}(h)=0$ approaching the traps. A similar section along line *B* downstream of the array demonstrates roughly 40% purification of both large and small spheres. Much of the background can be attributed to large particles escaping from the weakest traps in our array [4]. In denser suspensions, this escape rate is increased by collisions. Both processes can be mitigated by projecting multiple lines of traps, with perfect deflection of the locked-in fraction having been demonstrated [4] at throughputs exceeding 10 000 particles/s. Larger arrays, thicker samples, and faster flows would facilitate much higher throughputs.

Optical fractionation's ability to distinguish objects arises as a general and previously unappreciated feature of transport through periodically structured environments. Analyzing such transport not only provides insights into optimizing practical sorting, but also sheds new light on a range of analogous processes.

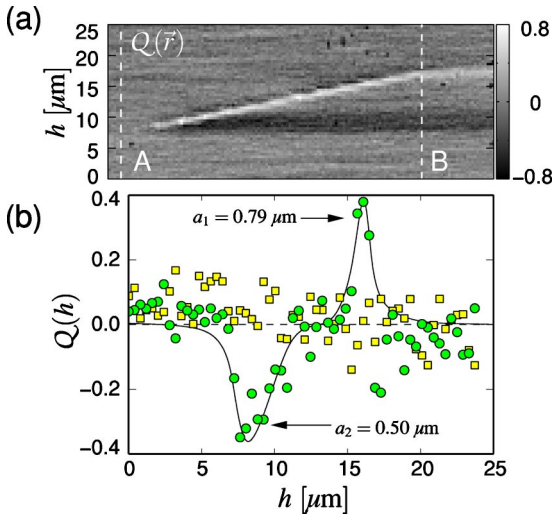

FIG. 3. (Color online) (a) Spatially resolved quality of separation $\mathcal{Q}(\boldsymbol{r})$ obtained with a single line of optical traps. The cross section transverse to the flow direction along line A is plotted as squares in (b) and provides a baseline profile for the suspension's composition before optical fractionation. The cross section along B [circles in (b)] shows the influence of the trap array. The curve in (b) is a guide to the eye.

The potential energy landscape presented by an optical trap array is a convolution of the traps' intensity profile $I(\boldsymbol{r})$ with an object's optical form factor $f(\boldsymbol{r})$: $V(\boldsymbol{r})=-I(\boldsymbol{r})\circ f(\boldsymbol{r})$. The total applied force then is $\boldsymbol{F}=\boldsymbol{\nabla}[I(\boldsymbol{r})\circ f(\boldsymbol{r})]+\boldsymbol{F}_0$, where $\boldsymbol{F}_0$ is the driving force. An overdamped particle's trajectory, $\boldsymbol{v}=\boldsymbol{F}/\gamma$, has one component, v_x, along the row of traps and another, v_y, perpendicular. Although this problem is well understood in one dimension [1], few analytic results are available for the inclined line, and fewer still incorporate thermal or quenched randomness. Consequently, we focus on the kinematic limit in which the driving and trapping forces dominate and trajectories may be treated deterministically. We then estimate the threshold for an object to escape from an array of optical traps, and thereby establish the selectivity of optical fractionation.

Any trajectory entrained by the traps, such as the example in Fig. 1(b), is characterized by turning points where $v_y=0$. Conversely, any trajectory without such turning points must be unbounded. This establishes as the maximum possible locked-in deflection angle

$$\sin\theta_m \leqslant \max\{\partial_y[-I(\boldsymbol{r})\circ f(\boldsymbol{r})]\}/F_0. \tag{1}$$

At a given θ, objects are either deflected or not with a selectivity set by the dependence of $\sin\theta_m$ on material properties. To estimate θ_m, we model the array as a periodically modulated line of light with intensity I_0:

$$I(\boldsymbol{r}) = I_0\, A(y)\sum_{n=0}^{\infty}\alpha_n\cos(nkx), \tag{2}$$

where $k=2\pi/b$, the dimensionless transverse distribution $A(y)$ is symmetrically peaked around $A(0)=1$, and the coef-

ficients α_n account for the tweezers' detailed structure with $\Sigma_n\ \alpha_n = 1$.

Convolving first along the x direction by applying the Fourier convolution theorem to each term in the sum, and then noting that $\cos nkx \leqslant 1$ yields

$$\sin\ \theta_m \leqslant \frac{V_0}{F_0}\max\left\{-\partial_y\left[A(y)\circ\sum_{n=0}^{\infty}\alpha_n\tilde{f}(nka,y)\right]\right\}, \quad (3)$$

where $V_0 \propto I_0$ is the potential wells' depth and $\tilde{f}(nka,y)$ is the form factor's Fourier transform along the x direction. The array's periodicity thus selects a discrete set of wave numbers from the continuous $\tilde{f}$ whose dependence on a endows optical fractionation with exceptional size selectivity. This is most clearly demonstrated if $\tilde{f}$ can be factored into inline and transverse components, $\tilde{f}(nka,y) = \tilde{f}_x(nka) f_y(y)$. In this case,

$$\sin\ \theta_m \leqslant q(a)\sum_{n=0}^{\infty}\alpha_n\tilde{f}_x(nka), \quad (4)$$

with $q(a) = \kappa(a)V_0/F_0$ and $\kappa(a) = \max\{-\partial_y[A(y)\circ f_y(y)]\}$. Equivalent results can be obtained when $\tilde{f}$ is not separable.

We turn our attention first to the transverse contribution. If a particle is comparable in size to the optical tweezers' width, w_0, then $\kappa(a)$ depends no more strongly on size than $1/a$. For example, if A and f_y are Gaussians of widths w_0 and a, respectively, then $\kappa(a) \propto 1/\sqrt{w_0^2 + a^2}$. Similarly, the potential depth V_0 and driving force F_0 generally scale as simple powers of a. Comparable algebraic sensitivity to size and material properties is offered by other techniques such as gel electrophoresis and field flow fractionation [7], and would be obtained with an unmodulated line of light ($\alpha_0 = 1$).

The in-line contribution is more interesting. Because a particle's form factor vanishes outside the interval $x \in [-a,a]$, its Fourier transform depends very strongly on wave number. For example, a uniform dielectric cube aligned with the array has a separable form factor, $f_x(x) = 1$ for $|x| < a$ whose Fourier transform, $\tilde{f}_x(ka) = \sin ka/(ka)$, is bounded by the leading-order cumulant expansion, $\tilde{f}_x(ka) \lesssim \exp(-k^2a^2/6)$. The equivalent result for a sphere [8] with $f(\boldsymbol{r}) = \sqrt{1 - r^2/a^2}$ for $|r| < a$ is $\tilde{f}_x(ka) \approx (\pi/2)\exp(-k^2a^2/8)$, and $f_y(y) \approx \exp(-k^2y^2/8)$. All of these bounding approximations surpass exponential selectivity for $ka \gtrsim 1$, with the actual form factors depending even more strongly on ka. Any smooth, bounded, positive-definite $f(\boldsymbol{r})$ on $x \in [-a,a]$ would behave similarly. Applying this insight to Eq. (4) establishes the lock-in transition's exponential size sensitivity for $ka \gtrsim 1$

Comparably strong dependence on control parameters is observed in analogous transitions between sub-harmonic steps in driven charge density waves [9] and between kinetically locked-in states in two-dimensional optical trap arrays [4]. Similar results also can be obtained for arrays of potential barriers, suggesting that arrays of optical tweezers also should be effective for sorting absorbing, reflecting and low-dielectric particles that are repelled by laser light. This analysis also carries over to filtration by arrays of micromachined posts [10], which therefore should be able to resolve objects substantially smaller than the inter-post separation.

Both $\tilde{f}(nka,y)$ and the coefficients α_n fall off rapidly with index n. Consequently, the sum in Eq. (4) is dominated by the first term, $n = 1$. This improves the approximations used in deriving Eq. (4) and suggests that the result may be considered an estimate for $\sin\ \theta_m$ rather than simply a bound.

To demonstrate this, we apply this analysis to our present experimental data, modeling the individual optical traps as Gaussian potential wells

$$V(\boldsymbol{r}) = V_0(a)\sum_{j=1}^{N}\exp\left(-\frac{(\boldsymbol{r} - jb\hat{x})^2}{2\sigma^2(a)}\right), \quad (5)$$

with $\sigma^2(a) \approx w_0^2 + a^2$ [11]. In this model,

$$\sin\ \theta_m \lesssim q(a)\exp\left(-\frac{b^2}{8\sigma^2}\right), \quad (6)$$

where $q(a) = (2/\sqrt{e})V_0/(\sigma F_0)$. The weakest trap's occupancy, n_j, is inversely proportional to the particles' minimum speed, $v_{\min}$, as they pass through. Consequently, we can estimate the relative trap strength from the data in Fig. 2 as $q(a) = 2(1 - v_{\min}/u)$. Similarly, the separation between the depleted region ahead of the traps and the position of maximum occupancy is $2\sigma(a)$. From the histograms in Figs. 2(c) and 2(d), we obtain $q(a) = 1.6 \pm 0.1$ and 0.9 ± 0.2, and $\sigma(a) = 0.85 \pm 0.07$ μm and 0.58 ± 0.07 μm for the large and small spheres, respectively [11]. These results suggest $\theta_m = 14° \pm 1° > \theta$ for the large spheres and $\theta_m = 3° \pm 2° \ll \theta$ for the small, which is consistent with the observation that only the large spheres are systematically deflected at $\theta = 12°$.

The threshold, $\sin\ \theta_m$, depends only linearly on V_0 and F_0. Thus, imperfections in practical trap arrays and fluctuations in the driving force can be largely compensated for by the substantially stronger dependence on particle size. Indeed, Figs. 2 and 3 demonstrate robust size separation despite more than 20% variation in flow velocity over the course of the experiment.

Equation (6) also offers insights into applying optical fractionation to nanometer-scale objects. Stokes drag scales linearly with a, and the optical trapping potential for Rayleigh particles scales as a^3, so that $q(a) \propto a^2$. Sorting proteins or nanoclusters, therefore, will require enhancing V_0 by four orders of magnitude. This might be accomplished by increasing the light's intensity and reducing its wavelength [12]. Even then, only algebraic size sensitivity should be expected for objects with $a \ll \lambda$ because $ka \ll 1$ in this limit. Exploiting resonances might overcome this limitation.

We have focused on effects due to deflection transverse to the optical axis. Multi-dimensional separations could take advantage of Bessel beams' ability to exert controlled axial forces [13] to distribute objects both transverse to and along the optical axis.

In summary, we have demonstrated optical fractionation for a model system of bidisperse colloidal spheres. This approach lends itself to continuous, rather than batch-mode fractionation, with continuous tuning and dynamic optimization over the entire accessible size range, i.e., nanometers to

micrometers. The abrupt transition from free flow to kinetically locked-in transport should offer exponential size selectivity for objects larger than roughly 100 nm. Separation on the basis of other characteristics also can be optimized, although exponential sensitivity should not be expected in general. Our analysis focuses on the kinematic limit, $F_0 b > V_0 > k_B T$, which is both tractable and appropriate for weakly-trapped micrometer-scale colloid. Stronger trapping would require a more detailed treatment of thermally assisted hopping [1]. A substantially more sophisticated analysis also would be required for higher-dimensional arrays.

The foregoing analysis may be applied to analogous systems. For example, we anticipate that similarly abrupt transitions should occur with variation of driving or trapping strength for vortex creep through patterned type-II superconductors [14], electron transport through two-dimensional electron gases [15], and electromigration on crystal surfaces, with potentially useful applications resulting in each case.

Note added. Recently, we have become aware of a subsequently submitted independent experimental study of colloidal sorting in an optical lattice [16].

We are grateful to Paul Chaikin and Matthew Pelton for enlightening discussions. This research was supported primarily by the National Science Foundation through Grant Nos. DMR-0304906 and DBI-0233971 and in part by the MRSEC and REU programs of the NSF through Grant No. DMR-0213745.

[1] H. Risken, *The Fokker-Planck Equation*, 2nd ed. (Springer-Verlag, Berlin, 1989).

[2] A. Ashkin, J. M. Dziedzic, J. E. Bjorkholm, and S. Chu, Opt. Lett. **11**, 288 (1986).

[3] E. R. Dufresne and D. G. Grier, Rev. Sci. Instrum. **69**, 1974 (1998); E. R. Dufresne, G. C. Spalding, M. T. Dearing, S. A. Sheets, and D. G. Grier, *ibid.* **72**, 1810 (2001); J. E. Curtis, B. A. Koss, and D. G. Grier, Opt. Commun. **207**, 169 (2002).

[4] P. T. Korda, M. B. Taylor, and D. G. Grier, Phys. Rev. Lett. **89**, 128301 (2002).

[5] J. C. Crocker and D. G. Grier, J. Colloid Interface Sci. **179**, 298 (1996).

[6] E. R. Dufresne, D. Altman, and D. G. Grier, Europhys. Lett. **53**, 264 (2001).

[7] *Encyclopedia of Separation Science*, edited by I. D. Wilson (Academic, San Diego, 2000).

[8] C. F. Bohren and D. R. Huffman, *Absorption and Scattering of Light by Small Particles* (Wiley Interscience, New York, 1983).

[9] S. E. Brown, G. Mozurkewich, and G. Grüner, Phys. Rev. Lett. **52**, 2277 (1984).

[10] T. A. J. Duke and R. H. Austin, Phys. Rev. Lett. **80**, 1552 (1997).

[11] This form applies in both Rayleigh ($a \ll w_0$) and ray-optics ($a \gg w_0$) limits [12], and is consistent with our measurements, assuming $w_0 \approx \lambda/2$.

[12] P. A. M. Neto and H. M. Nussenzveig, Europhys. Lett. **50**, 702 (2000).

[13] J. Arlt, V. Garces-Chavez, W. Sibbett, and K. Dholakia, Opt. Commun. **197**, 239 (2001).

[14] C. Reichhardt and F. Nori, Phys. Rev. Lett. **82**, 414 (1999).

[15] J. Wiersig and K.-H. Ahn, Phys. Rev. Lett. **87**, 026803 (2001).

[16] M. P. MacDonald, G. C. Spalding, and K. Dholakia, Nature (London) **426**, 421 (2003). See K. Ladavac, M. Pelton, and D. G. Grier, e-print cond-mat/0404242 for a critical discussion of the alternative sorting mechanism proposed in this paper.